SUPPLEMENTAL INFORMATION

Mitochondrial membrane potential identifies cells with enhanced stemness for cellular therapy

Madhusudhanan Sukumar[1]*, Jie Liu[2], Gautam U. Mehta[1], Shashank J. Patel[1,3], Rahul Roychoudhuri[1], Joseph G. Crompton[1], Christopher A. Klebanoff[1,4], Yun Ji[5], Peng Li[6], Zhiya Yu[1], Greg D. Whitehill[7], David Clever[1,8], Robert L Eil[1], Douglas Palmer[1], Suman Mitra[6], Mahadev Rao[9], Keyvan Keyvanfar[7], David Schrump[9], Ena Wang[10], Francesco Marincola[10], Luca Gattinoni[5], Warren J Leonard[6], Pawel Muranski[7], Toren Finkel[2] and Nicholas P. Restifo[1]*

[1]Center for Cancer Research, National Cancer Institute (NCI), National Institutes of Health, Bethesda (NIH), MD, 20892 USA.
[2]Center for Molecular Medicine, National Heart, Lung, and Blood Institute (NHLBI), NIH, Bethesda, MD, 20892 USA.
[3]NIH-Georgetown University Graduate Partnership Program, Georgetown University Medical School, Washington, DC 20057, USA.
[4] Clinical Investigator Development Program, NCI, NIH, Bethesda, MD, 20892 USA.
[5]Experimental Transplantation and Immunology Branch, NCI, NIH, Bethesda, MD, 20892 USA.
[6]Laboratory of Molecular Immunology and the Immunology Center, NHLBI, NIH, Bethesda, MD, 20892 USA.
[7]Hematology Branch, NHLBI, NIH, Bethesda, MD, 20892 USA.
[8]Medical Scientist Training Program, The Ohio State University College of Medicine, Columbus, OH, 43210 USA
[9]Thoracic and GI Oncology Branch, NCI, NIH, Bethesda, MD, 20892 USA.
[10]Sidra Medical and Research Center, Doha, Qatar

*Correspondence: M.S. (sukumarm2@mail.nih.gov) or N.P.R. (restifo@nih.gov).

Supplemental Figures

Figure S1, related to Figure 1. Phenotypic and functional characterization of low-Δψm and high-Δψm CD8$^+$ T cells

(A) Post-sort flow cytometric of CD8$^+$ T cells confirmed the separation of discrete populations based on Δψm. (B) Flow cytometric analysis of sorted low-Δψm, high-Δψm and naïve CD8$^+$ T cells based on conventional markers of differentiation (CD44, CD27 and IL7Rα), activation (CD69) and senescence (KLRG1), (C) Flow cytometric analysis of CD62L expression (D) Quantification of CD62L expression (E) MFI of low-Δψm and high-Δψm cells expressing perforin (F) MFI of low-Δψm and high-Δψm cells expressing Granzyme B (G) Ki-67 expression in sorted low-Δψm and high-Δψm (H) Flow cytometric analysis of CD8$^+$ T cells in the spleen after adoptive transfer of 1 X 10^5 high and low-Δψm cells and subsequent infection with gp100-vaccinia virus in sub-lethally irradiated mice (lymphodepleted host). Frequency of transferred cells (Thy1.1$^+$) was assessed on day 3, day 5 and day 7 after transfer. (I) Effector cytokine production was measured in high and low-Δψm-sorted subsets at day 5 during the peak of expansion in lymphodepleted host. Data are presented as mean ± SEM and **** = $P < 0.0001$ (two-tailed t test).

Table S1, related to Figure 1. List of differentially expressed genes between Tscm and Tem CD8$^+$ T cells

Mouse Tscm and Tem CD8$^+$ T cell subsets were generated and the microarray analysis was performed and the list of differentially expressed genes was shown.

Figure S2, related to Figure 2. Metabolic characterization of low-Δψm and high-Δψm CD8$^+$ T cells.

(A) Relative ribose-5-phosphate, ribulose-5-phosphate and sedoheptulose-5-phosphate levels were measured in the low and high T cell subsets using LC/MS. (B) Quantitative RT-PCR analysis was performed for the expression of hexokinase-2 (*Hk2*), lactate dehydrogenase-A (*Ldha*) and pyruvate dehydrogenase kinase-2 (*Pdk2*) was measured in high and low Δψm–sorted subsets (relative to *Actb* mRNA levels, mean ± s.e.m. of 3 measurements). (C) Basal oxygen consumption rate (OCR) was measured in high and low Δψ–sorted subsets (mean ± s.e.m. of 4 measurements). Data are presented as mean ± SEM and ** = P < 0.01 (two-tailed t test). * = P < 0.05; ** = P < 0.01; *** = P < 0.001; (two-tailed t test).

Table S2, related to Figure 2. List of differentially expressed genes between low-Δψm and high-Δψm CD8$^+$ T cells

Pmel-1 CD8$^+$ T cells were activated for three days and the low-Δψm and high-Δψm CD8$^+$ T cells subsets were sorted and the RNA-seq analysis was performed. The list of differentially expressed genes between the low-Δψm and high-Δψm were shown.

Figure S3, related to Figure 3. Mitochondrial membrane potential (Δψm)-based sorting in central memory T cell subset (T_{CM}) and gene expression profile of Δψm T_{CM} subsets.

(A) Schema for Δψm sorting by TMRM fluorescence in T_{CM} cells. (B) Post-sort flow cytometry of CD8$^+$ T cells confirmed the separation of discrete populations based on Δψm. (C) Central memory CD8$^+$ T cells were sorted for mitochondrial membrane potential as shown in Supplementary Figure S3A and quantitative RT-PCR analysis was performed for the expression of representative memory ,effector and metabolic genes in CD8$^+$ T cells sorted as in supplementary figure S3A (relative to *Actb* mRNA levels, mean ± s.e.m. of 3 measurements).(D) Post-sort flow cytometry of Tc17 CD8$^+$ T cells confirmed the separation of discrete populations based on Δψm. Data are representative of two independent experiments. Data are presented as mean ± SEM and ** = P < 0.01; *** = P < 0.001; **** = P < 0.0001 (two-tailed t test).

Figure S4, related to Figure 3. Mitochondrial membrane potential based sorting and characterization of ΔΨm subsets in LT-HSC and bulk $CD8^+$ T cells.

(A) Flow cytometric analysis of c-Kit^+ $Sca1^+$ Lin^- (KSL) cells within mouse bone marrow and sorting strategy of Lin^- c-Kit^+ Sca-1^+ cells based on TMRM into low-ΔΨm HSC and high-ΔΨm HSC (B) Phenotypic characterization of low-ΔΨm HSC and high-ΔΨm HSC based on c-Kit and CD150 surface markers (C) Quantification of CD150 positive KSL cells in low-ΔΨm HSC and high-ΔΨm HSC (D) Flow cytometric analysis for reactive oxygen species (ROS) levels using 2',7' –dichlorofluorescein diacetate (DCFDA) fluorescence expressed in arbitrary units (AU) demonstrating reduced ROS levels in $CD8^+$ T cells after treatment with 5 μM carbonyl cyanide-4-(trifluoromethoxy)phenylhydrazone (FCCP) (E) Relative glutathione levels were measured in the low-Δψm and high-Δψm T cell subsets using LC/MS (F) By quantitative RT-PCR analysis, antioxidant gene expression was noted to be higher in the low-Δψm cells. Data are presented as mean ± SEM and * = $P < 0.05$; ** = $P < 0.01$; *** = $P < 0.001$; (two-tailed t test).

Figure S5, related to Figure 5. Interleukin-2 augments mitochondrial membrane potential through mTOR signaling

(A) Basal oxygen consumption rate (OCR) and OCR/ECAR ratio measured in activated T cells grown in various concentrations of IL-2 (B) Flow cytometric analysis of activated T cells for mitochondrial membrane potential (Δψm) demonstrated a dose-dependent influence of IL-2 on ΔΨm (C) Flow cytometric based characterization of mTOR signaling in Δψm subsets revealed that low-ΔΨm T cells display reduced mTOR activity (D) mitochondrial membrane potential (ΔΨm) in activated T cells was measured in the presence or absence of rapamycin. Data are presented as mean ± SEM and * = $P < 0.05$; **** = $P < 0.0001$ (two-tailed t test).

Supplemental Experimental Procedures

In vitro activation of T cells. $CD8^+$ T cells from C57BL/6 mice were stimulated using plate-bound anti-CD3 (2 µg/ml; 145-2C11; BD Biosciences) and soluble anti-CD28 (1 µg/ml; 37.5 l; BD Biosciences) and expanded in culture medium containing 10 ng•ml–1 IL-2 (Chiron) for 4 days. $CD8^+$ T cells from pmel-1 mice were stimulated in vitro with 1 µM hgp$100_{25–33}$ peptide or plate-bound anti-CD3 and soluble anti-CD28 and expanded in culture medium containing 10 ng•ml–1 IL-2 (Chiron) for 4 days. In select experiments, $CD8^+$ T cells were cultured in presence of an mTOR inhibitor (100ng/ml rapamycin; Sigma-Aldrich). Similarly, $CD8^+$ T cells were stimulated using plate bound anti-CD3 and soluble anti-CD28 either in the absence and presence of FCCP (Sigma-Aldrich).

Microarray data collection and analysis. The T_{SCM} and T_{EM} subsets were generated as previously described (Gattinoni et al., 2009). Microarray data collection and analysis was performed as previously described (Crompton et al., 2015). Microarray data comparing the T_{SCM} and T_{EM} subsets are available in NCBI GEO database under accession number GSE67825.

$CD8^+$ T cells antibodies and flow cytometry. Mouse antibodies specific for CD8α (53-6.7), IL7Rα (A7R34), Thy-1.1 (OX-7), CD44 (IM7), CD62L (MEL-14), CD27 (LG.3A10), and KLRG-1 (2F1) were purchased from BD Biosciences. Mouse antibody specific for CD69 (H1.2F3) were obtained from eBioscience. Mouse antibodies for T cell exhaustion markers for PD-1 and LAG-3 were purchased from eBioscience and antibodies for CTLA-4 was purchased from Biolegend. FACS Canto I or FACS Canto II (BD Biosciences) was used for flow cytometry acquisition. Samples were analyzed with FlowJo software (TreeStar). For the Flow Cytometric analysis of apoptotic population in T cells, we used FITC Annexin V staining kit from BD Pharmigen.

Enumeration of adoptively transferred cells. We euthanized mice at the indicated time points after infection. Splenocytes were enumerated by trypan blue exclusion. The frequency of transferred T cells was determined by measuring $CD8^+$ and Thy-1.1 with flow cytometry. The

absolute number of pmel-1 cells was calculated by multiplying the total cell count by the percent $CD8^+$ Thy-1.1^+.

Generation and metabolic-sorting of central-memory T_{CM}, Tc17, Th1 and Th17 cells.

$CD8^+$ T cells from pmel-1 mice were stimulated in vitro with 1 μM $hgp100_{25–33}$ peptide and expanded for 4 days in culture. After 4 days, cells were stained with CD62L and CD44 using an initial gating strategy based on T_{CM} surface markers (gated on $CD8^+CD44^+CD62L^+$). For sorting of central-memory populations with different mitochondrial membrane potential, we further partitioned the T_{CM} cells into two pools corresponding to the cells with the lowest (7-10%) low-ΔΨm T_{CM} and highest (7-10%) high-ΔΨm T_{CM} TMRM fluorescence. Cell sorting was performed on with a FACS Aria instrument (BD Biosciences).

Type 17 skewing was accomplished by priming pmel-1/Thy1.1 splenocytes with 1 μM $hgp100_{25-33}$ in rmIL-6 (5 ng/mL) and recombinant human transforming growth factor-β (rhTGF-β; 10 ng/mL; R&D Systems), and anti–IFN-γ (10 μg/mL; eBioscience). Beginning 2 days after priming, cell cultures were expanded with rhIL-2 (30 IU/mL; Novartis). Control cells were primed and expanded with IL-2 alone (Hinrichs et al., 2009). Mitochondrial activity based membrane potential was assessed using TMRM at a final concentration of 25 nm for 30 min at room temperature. Sorting of Tc17 cells with different mitochondrial membrane potential, was performed as above. Naïve $CD4^+$ T cells were polarized into Th1 or Th17 subsets as previously described (Muranski et al., 2011).

LT-HSCs and mitochondrial membrane potential. Total bone marrow cells from CD45.1 congenic mice were stained with antibodies against lineage markers (CD3, CD4, CD8, Gr-1, Mac-1, Ter 119 and CD45R/B220, CD34, CD11b, CD150 (BD-Biosciences) Sca-1, c-kit (eBioscience) and CD34 (BioLegend) for 30 min at 40C then followed by staining with TMRM at a final concentration of 25 nM for 30 min at 37° C. Purified Lin^- $Sca1^+$ $c\text{-}Kit^+$ /$CD34^-$ cells were

sorted into two fractions corresponding to the lowest (10%) and highest (10%) levels of TMRM fluorescence using an excitation wavelength of 488nm. Transplantation was performed as previously described using either 300 high or low membrane potential Lin^- $Sca1^+$ $c\text{-}Kit^+$ /$CD34^-$ cells along with $3X10^5$ competitor total bone marrow cells (CD45.2) into lethally-irradiated recipients (CD45.2).

Intracellular staining and flow cytometry. The following antibodies were from Cell Signaling: The intracellular staining for phosphorylated mTOR, pS6 and p4EBP1 was performed as previously described (Rao et al., 2010) using antibodies directed against S6 ribosomal protein phosphorylated at Ser 235/236(D57.2.2E) (4803) (Cell Signaling). A 1:1,000 dilution was used for all antibodies. For the effector lineages (Tc17, Th1 and Th17 cell cultures), the intracellular staining for the detection of cytokines such as IL-17 A, IL-17F and IFN-γ was as previously described (Muranski et al., 2011).

H2AX DNA-damage foci staining. Cells were fixed with 4% paraformaldehyde and permeabilized with 0.25% Triton X-100. Cells were incubated for 1 hour in blocking buffer composed of 5% BSA in PBS and then incubated with mouse monoclonal anti-γ-H2AX antibody (1: 1000, , Millipore, Temecula CA) overnight at 4 ºC, followed by secondary Alexa-488-conjugated anti-mouse IgG (1:1000 Jackson ImmunoResearch Laboratories, IncWest Grove, PA). Percentages of γ-H2AX positive cells (cells with > 3 H2AX foci per nuclei were termed positive) were obtained by randomly counting 300 cells (n=3 independent experiments). For the flow cytometric analysis of H2AX in lymphocytes and LT-HSC, we used phospho-Histone H2A.X (Ser139) antibody (Cell Signaling).

RNA Sequencing. $CD8^+$ T cells from pmel-1 mice were stimulated in vitro with 1 μM hgp10025–33 peptide and expanded in culture medium containing 10 ng•ml–1 IL-2 (Chiron) for 4 days. Cells were sorted based on TMRM fluorescence and total RNA was isolated from low-

ΔΨm and high-ΔΨm subsets. Later cDNA was synthesized with 2.5 ng of the pooled RNA and amplified by a two-step PCR process. After fragmentation with a Bioraptor (Diagenode), fragments 220–400 base pairs in length were isolated with 2% E-Gel (Invitrogen), then ends were repaired and an adaptor (Illumina) was added with T4 DNA ligase (New England Biolabs), followed by amplification for seventeen cycles with PE 1.0 and PE 2.0 primers (Illumina) and Phusion High Fidelity PCR Master Mix (New England Biolabs). PCR products were 'barcoded' (indexed) and sequenced on an Illumina HiSeq 2000 platform.

RNA sequencing data analysis. Sequenced reads (single-end 36 base pairs) were aligned to the RefSeq mouse gene database (mm8 revision) with the ELAND pipeline. Raw reads that fell on exons of each gene were counted and normalized reads per kilobase of exon model per million mapped reads were calculated for each gene. The statistical packages in software R (The R Foundation for Statistical Computing, Austria, Vienna) were used for multidimensional scaling, linear-regression modeling and analysis of differences in gene expression.

Ocular autoimmunity. For ocular autoimmunity evaluation, eyes were enucleated 300 days after adoptive transfer, fixed in 10% formalin, embedded in methylacrylate, sectioned via papillary-optic nerve axis, H&E-stained, and autoimmunity assessed in a blinded fashion. The ocular autoimmune score represents the sum of iridiocyclitis, choroiditis, and vitritus using the following scoring method: none = 0, mild = 1, moderate = 2 and severe = 3. Values are presented as mean ± SEM. For assessment of vitiligo, We used the following scoring system: 0 = none, 1 = trace, 2= 25-50% coat involved, 3= 50-75% coat involved, 4=>75% coat involved, 5=full coat involvement. Values are presented as mean ± SEM.

Metabolomics. Using a FACS Aria instrument (BD Biosciences) we sorted TMRM-high and TMRM-low subsets of $CD8^+$ T cells pmel-1 $CD8^+$ T cells 5 days after activation with cognate

hgp100$_{25–33}$ peptide. Six biological replicates of TMRM-high and TMRM-low subsets were analyzed. Samples were split for separate analysis on GC/MS and LC/MS/MS platforms.

Sample Accessioning. Each sample received was accessioned into the Metabolon LIMS system and was assigned by the LIMS a unique identifier that was associated with the original source identifier only. This identifier was used to track all sample handling, tasks, results etc. The samples (and all derived aliquots) were tracked by the LIMS system. All portions of any sample were automatically assigned their own unique identifiers by the LIMS when a new task is created; the relationship of these samples is also tracked. All samples were maintained at -80 ºC until processed.

Metabolite analysis. Metabolomic profiling analysis was performed by Metabolon as previously described (Evans et al., 2009; Reitman et al., 2011)

Metabolite Sample Preparation. Samples were prepared using the automated MicroLab STAR® system from Hamilton Company. A recovery standard was added prior to the first step in the extraction process for QC purposes. Sample preparation was conducted using aqueous methanol extraction process to remove the protein fraction while allowing maximum recovery of small molecules. The resulting extract was divided into four fractions: one for analysis by UPLC/MS/MS (positive mode), one for UPLC/MS/MS (negative mode), one for GC/MS, and one for backup. Samples were placed briefly on a TurboVap® (Zymark) to remove the organic solvent. Each sample was then frozen and dried under vacuum. Samples were then prepared for the appropriate instrument, either UPLC/MS/MS or GC/MS.

Ultra high performance liquid chromatography/Mass Spectroscopy (UPLC/MS/MS). The LC/MS portion of the platform was based on a Waters ACQUITY ultra-performance liquid chromatography (UPLC) and a Thermo-Finnigan linear trap quadrupole (LTQ) mass spectrometer, which consisted of an electrospray ionization (ESI) source and linear ion-trap

(LIT) mass analyzer. The sample extract was dried then reconstituted in acidic or basic LC-compatible solvents, each of which contained 8 or more injection standards at fixed concentrations to ensure injection and chromatographic consistency. One aliquot was analyzed using acidic positive ion optimized conditions and the other using basic negative ion optimized conditions in two independent injections using separate dedicated columns. Extracts reconstituted in acidic conditions were gradient eluted using water and methanol containing 0.1% formic acid, while the basic extracts, which also used water/methanol, contained 6.5mM Ammonium Bicarbonate. The MS analysis alternated between MS and data-dependent MS2 scans using dynamic exclusion. Raw data files are archived and extracted as described below.

Gas chromatography/Mass Spectroscopy (GC/MS). The samples destined for GC/MS analysis were re-dried under vacuum desiccation for a minimum of 24 hours prior to being derivatized under dried nitrogen using bistrimethyl-silyl-triflouroacetamide (BSTFA). The GC column was 5% phenyl and the temperature ramp was from 40° to 300° C in a 16 minute period. Samples were analyzed on a Thermo-Finnigan Trace DSQ fast-scanning single-quadrupole mass spectrometer using electron impact ionization. The instrument was tuned and calibrated for mass resolution and mass accuracy on a daily basis. The information output from the raw data files was automatically extracted as discussed below.

Quality assurance/QC. For QA/QC purposes, additional samples were included with each day's analysis. These samples included extracts of a pool of well-characterized human plasma, extracts of a pool created from a small aliquot of the experimental samples, and process blanks. QC samples were spaced evenly among the injections and all experimental samples were randomly distributed throughout the run. A selection of QC compounds was added to every sample for chromatographic alignment, including those under test. These compounds were carefully chosen so as not to interfere with the measurement of the endogenous compounds.

Data extraction and compound identification. Raw data was extracted, peak-identified and QC processed using Metabolon's hardware and software. These systems are built on a web-service platform utilizing Microsoft's .NET technologies, which run on high-performance application servers and fiber-channel storage arrays in clusters to provide active failover and load-balancing. Compounds were identified by comparison to library entries of purified standards or recurrent unknown entities.

Statistics. Data sets were compared using 1- or 2-tailed unpaired Student's t test. The products of perpendicular tumor diameters were plotted as the mean ± SEM for each data point and tumor treatment graphs were compared by using the Wilcoxon rank sum test. For all analyses, a P value less than 0.05 was considered statistically significant. Prism GraphPad software (GraphPad Software Inc.) was used for these analyses. For HSC in vivo reconstitution, we used a 2-way ANOVA to compare treatment groups.

Study approval. All animal experiments were conducted with the approval of the National Cancer Institute Animal Use and Care Committee.

SUPPLEMENTAL REFERENCES

Crompton, J.G., Narayanan, M., Cuddapah, S., Roychoudhuri, R., Ji, Y., Yang, W., Patel, S.J., Sukumar, M., Palmer, D.C., Peng, W., et al. (2015). Lineage relationship of CD8 T cell subsets is revealed by progressive changes in the epigenetic landscape. Cellular & molecular immunology.

Evans, A.M., DeHaven, C.D., Barrett, T., Mitchell, M., and Milgram, E. (2009). Integrated, nontargeted ultrahigh performance liquid chromatography/electrospray ionization tandem mass spectrometry platform for the identification and relative quantification of the small-molecule complement of biological systems. Analytical chemistry *81*, 6656-6667.

Gattinoni, L., Zhong, X.S., Palmer, D.C., Ji, Y., Hinrichs, C.S., Yu, Z., Wrzesinski, C., Boni, A., Cassard, L., Garvin, L.M., et al. (2009). Wnt signaling arrests effector T cell differentiation and generates CD8+ memory stem cells. Nature medicine *15*, 808-813.

Hinrichs, C.S., Kaiser, A., Paulos, C.M., Cassard, L., Sanchez-Perez, L., Heemskerk, B., Wrzesinski, C., Borman, Z.A., Muranski, P., and Restifo, N.P. (2009). Type 17 CD8+ T cells display enhanced antitumor immunity. Blood *114*, 596-599.

Muranski, P., Borman, Z.A., Kerkar, S.P., Klebanoff, C.A., Ji, Y., Sanchez-Perez, L., Sukumar, M., Reger, R.N., Yu, Z., Kern, S.J., et al. (2011). Th17 cells are long lived and retain a stem cell-like molecular signature. Immunity *35*, 972-985.

Rao, R.R., Li, Q., Odunsi, K., and Shrikant, P.A. (2010). The mTOR kinase determines effector versus memory CD8+ T cell fate by regulating the expression of transcription factors T-bet and Eomesodermin. Immunity *32*, 67-78.

Reitman, Z.J., Jin, G., Karoly, E.D., Spasojevic, I., Yang, J., Kinzler, K.W., He, Y., Bigner, D.D., Vogelstein, B., and Yan, H. (2011). Profiling the effects of isocitrate dehydrogenase 1 and 2 mutations on the cellular metabolome. Proceedings of the National Academy of Sciences of the United States of America *108*, 3270-3275.

van der Windt, G.J., Everts, B., Chang, C.H., Curtis, J.D., Freitas, T.C., Amiel, E., Pearce, E.J., and Pearce, E.L. (2012). Mitochondrial respiratory capacity is a critical regulator of CD8+ T cell memory development. Immunity *36*, 68-78.

Figure S1

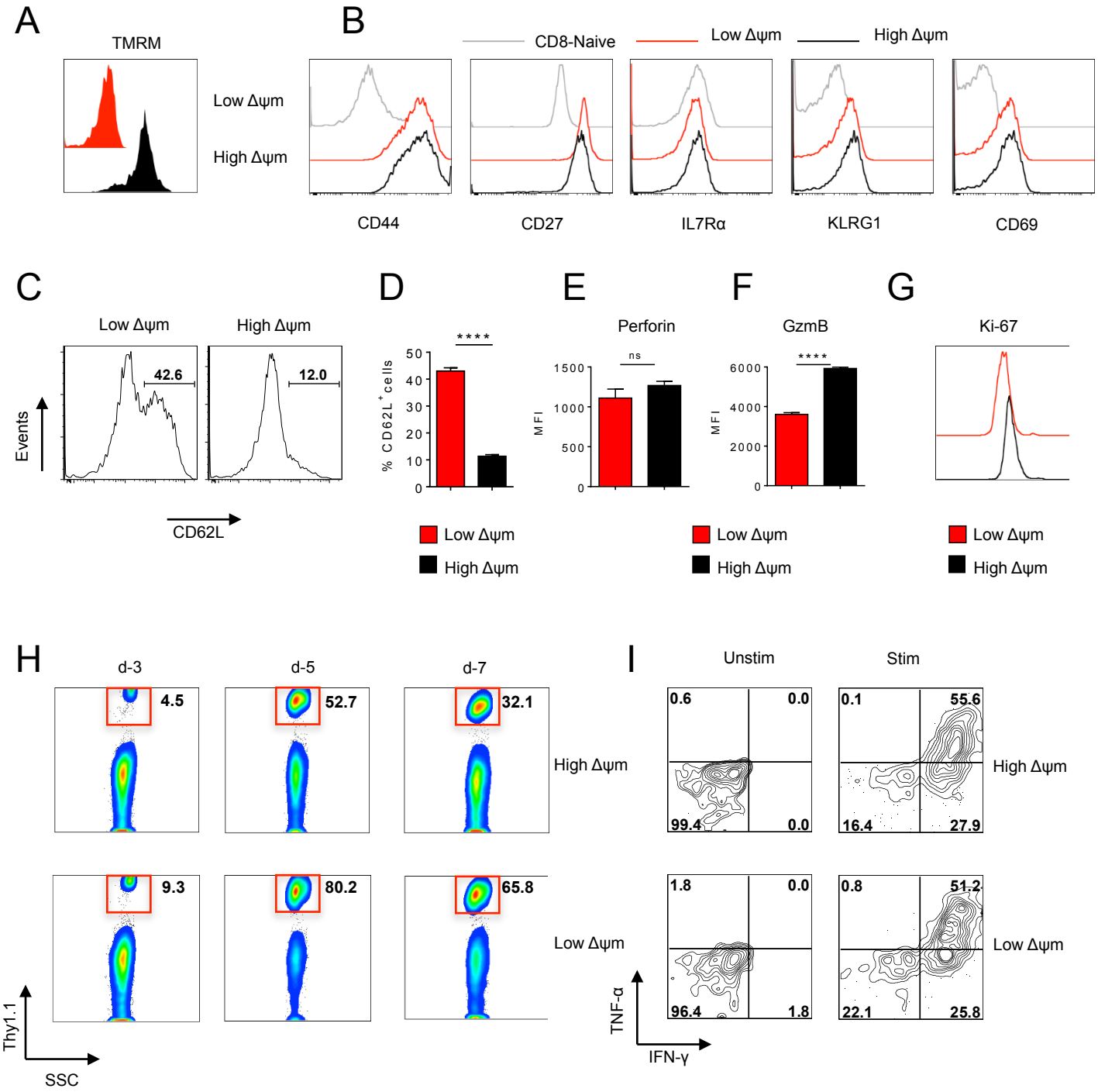
A
TMRM
Low Δψm
High Δψm
B
CD8-Naive
Low Δψm
High Δψm
CD44
CD27
IL7Rα
KLRG1
CD69
C
Low Δψm
High Δψm
42.6
12.0
Events
CD62L
D
****
% CD62L+ cells
50
40
30
20
10
0
Low Δψm
High Δψm
E
Perforin
ns
MFI
1500
1000
500
0
Low Δψm
High Δψm
F
GzmB
****
MFI
6000
4000
2000
0
Low Δψm
High Δψm
G
Ki-67
Low Δψm
High Δψm
H
d-3
d-5
d-7
4.5
52.7
32.1
High Δψm
9.3
80.2
65.8
Low Δψm
Thy1.1
SSC
I
Unstim
Stim
0.6
0.0
99.4
0.0
0.1
55.6
16.4
27.9
High Δψm
1.8
0.0
96.4
1.8
0.8
51.2
22.1
25.8
Low Δψm
TNF-α
IFN-γ

Figure S2

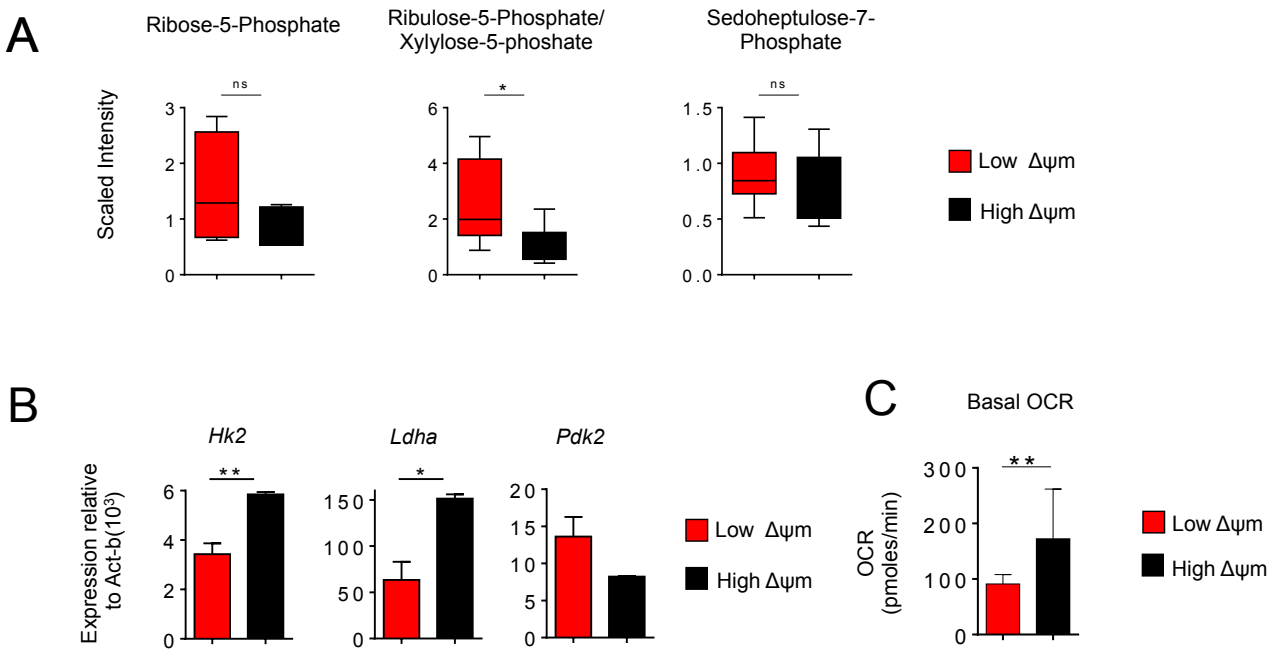
A
Ribose-5-Phosphate
Ribulose-5-Phosphate/
Xylylose-5-phoshate
Sedoheptulose-7-
Phosphate
Scaled Intensity
ns
*
ns
Low Δψm
High Δψm
B
Hk2
Ldha
Pdk2
Expression relative
to Act-b(10³)
**
*
Low Δψm
High Δψm
C
Basal OCR
OCR
(pmoles/min)
**
Low Δψm
High Δψm

Figure S3

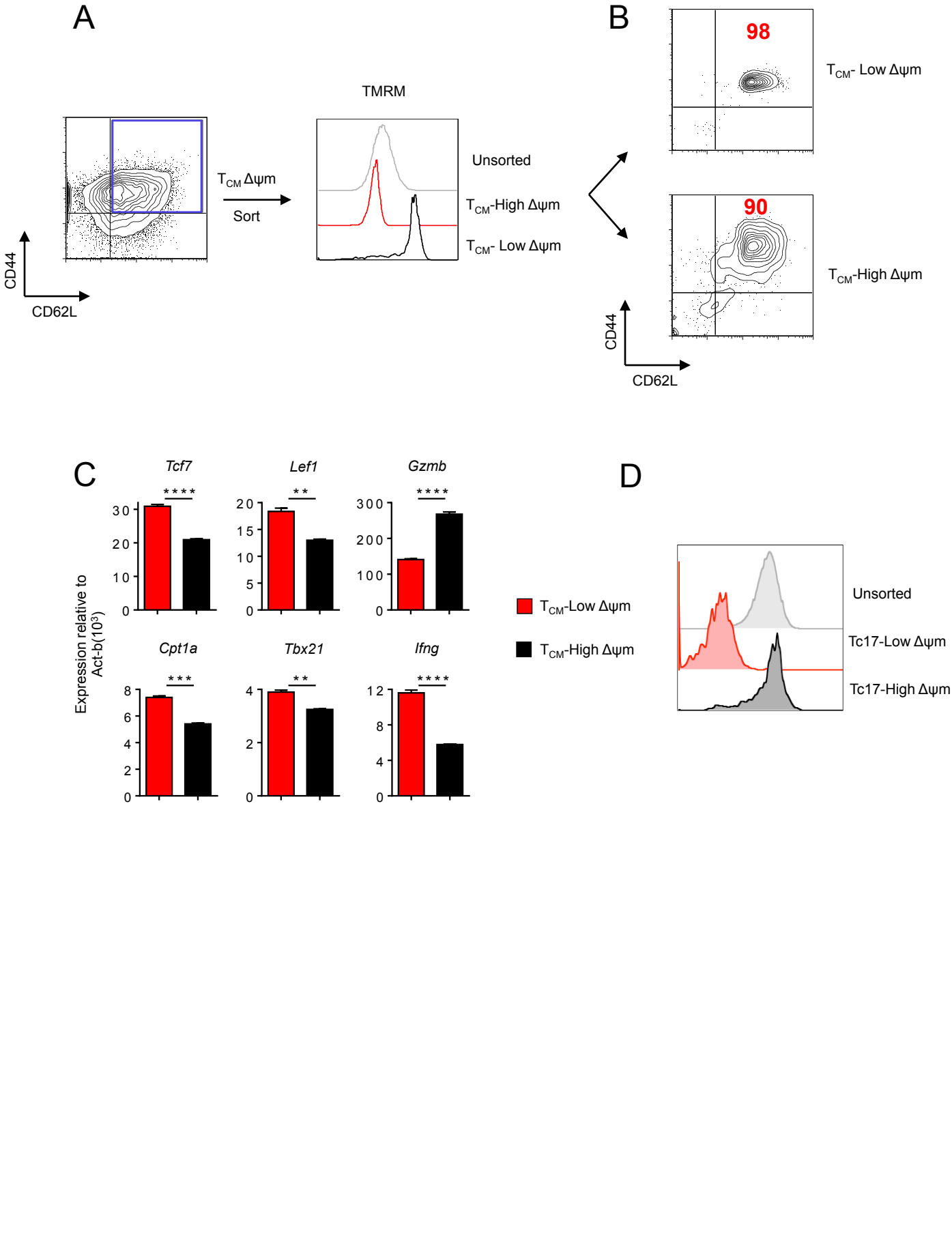
A
TMRM
CD44
CD62L
TCM Δψm
Sort
Unsorted
TCM-High Δψm
TCM- Low Δψm
B
98
90
TCM- Low Δψm
TCM-High Δψm
CD44
CD62L
C
Tcf7
Lef1
Gzmb
Cpt1a
Tbx21
Ifng
Expression relative to Act-b(10³)
TCM-Low Δψm
TCM-High Δψm
D
Unsorted
Tc17-Low Δψm
Tc17-High Δψm

Figure S4

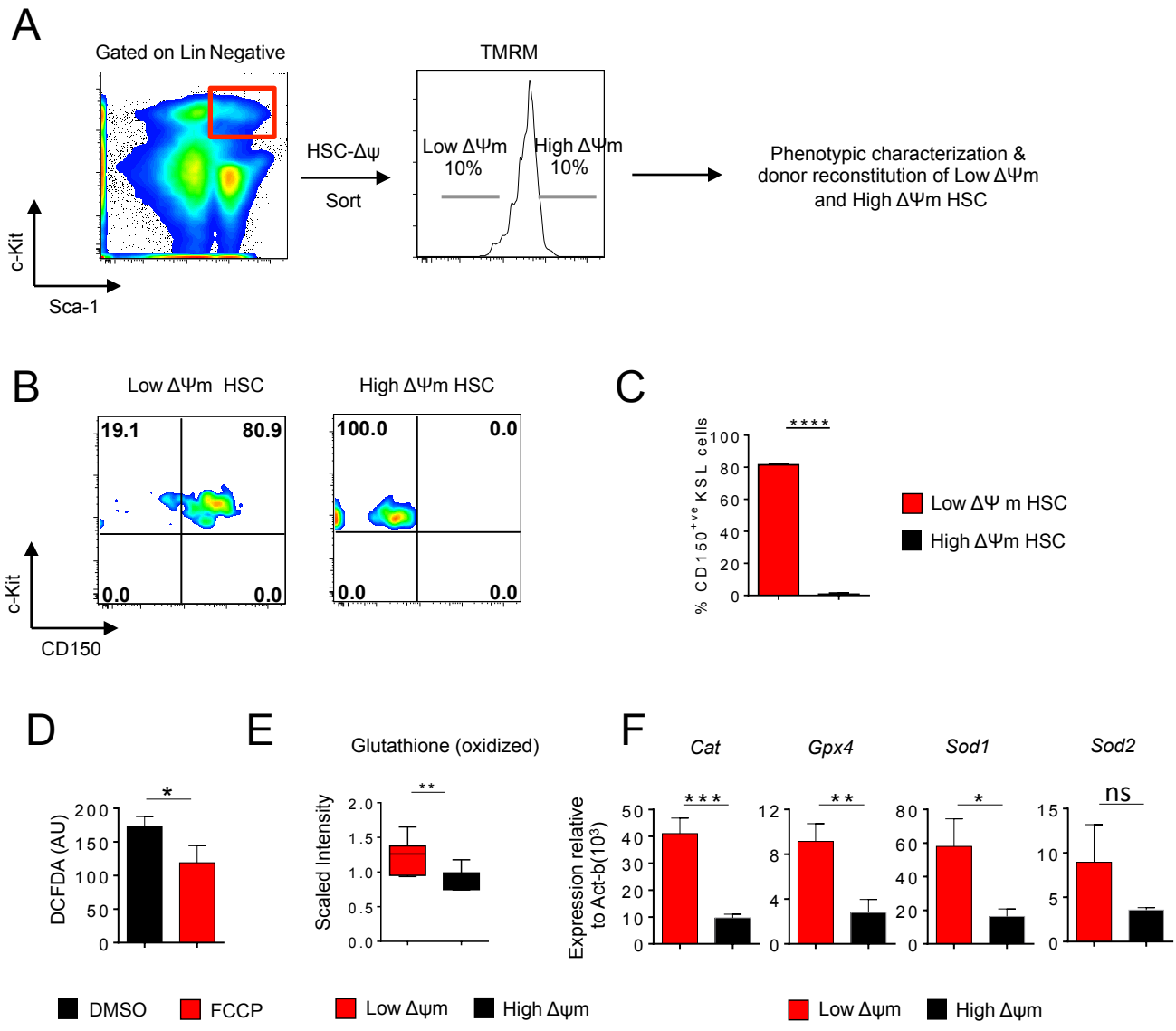
A
Gated on Lin Negative
c-Kit
Sca-1
HSC-Δψ
Sort
TMRM
Low ΔΨm 10%
High ΔΨm 10%
Phenotypic characterization & donor reconstitution of Low ΔΨm and High ΔΨm HSC
B
Low ΔΨm HSC
High ΔΨm HSC
19.1
80.9
0.0
0.0
100.0
0.0
0.0
0.0
c-Kit
CD150
C
% CD150+ve KSL cells
****
Low ΔΨ m HSC
High ΔΨm HSC
D
DCFDA (AU)
*
DMSO
FCCP
E
Glutathione (oxidized)
Scaled Intensity
**
Low Δψm
High Δψm
F
Cat
Gpx4
Sod1
Sod2
Expression relative to Act-b(10³)
***
**
*
ns
Low Δψm
High Δψm

Figure S5

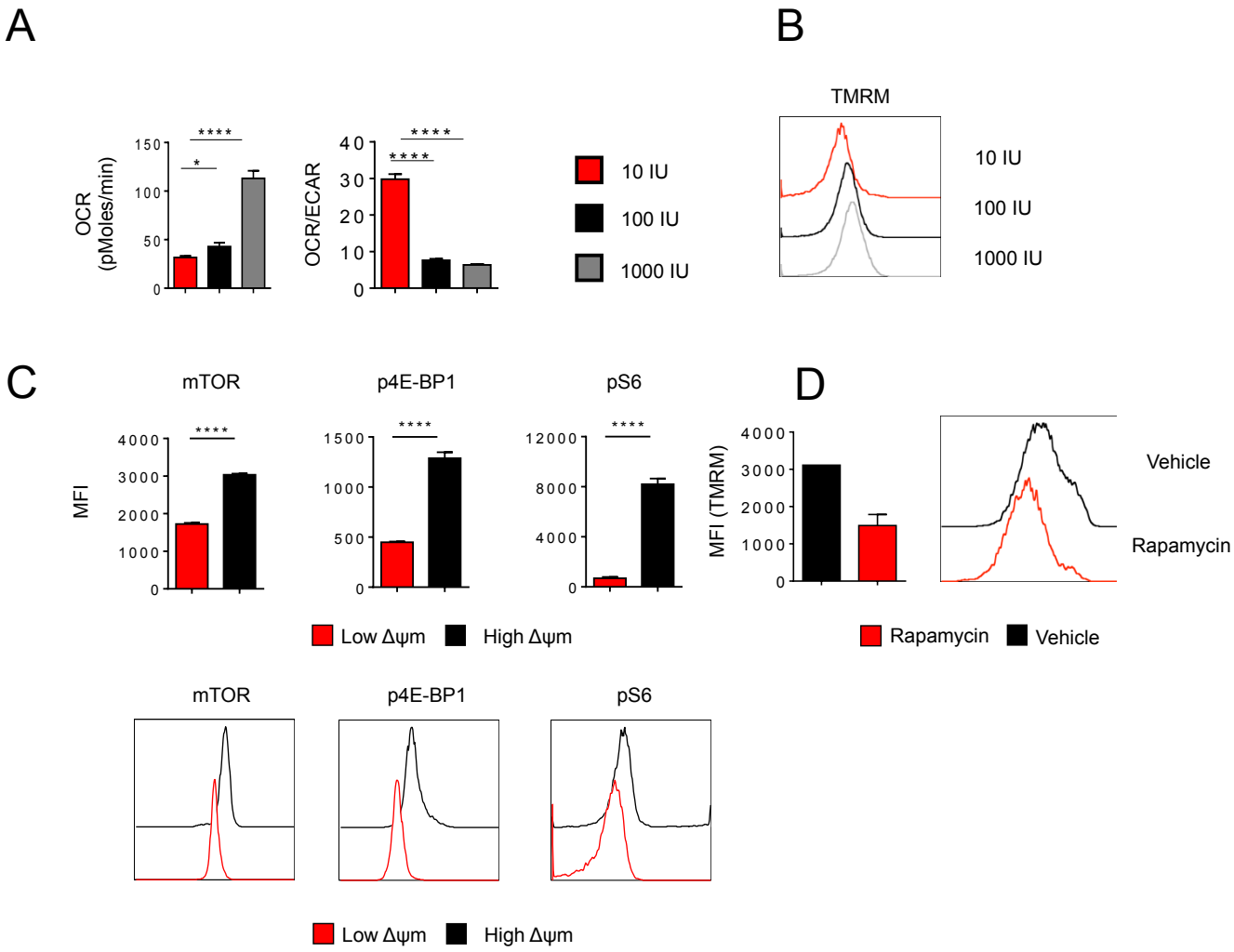
A
OCR (pMoles/min)
150
100
50
0
****
*
OCR/ECAR
40
30
20
10
0
****
****
10 IU
100 IU
1000 IU
B
TMRM
10 IU
100 IU
1000 IU
C
mTOR
p4E-BP1
pS6
MFI
4000
3000
2000
1000
0
1500
1000
500
0
12000
8000
4000
****
Low Δψm
High Δψm
D
MFI (TMRM)
4000
3000
2000
1000
0
Vehicle
Rapamycin
Rapamycin
Vehicle
mTOR
p4E-BP1
pS6
Low Δψm
High Δψm